American Mineralogist, Volume 66, pages 350–357, 1981

Single crystal X-ray refinement of pyrophyllite-1*Tc*

JUNG HOO LEE[1] AND STEPHEN GUGGENHEIM

Department of Geological Sciences
University of Illinois at Chicago
Chicago, Illinois 60680

Abstract

The crystal structure of pyrophyllite from Ibitiara, Bahia, Brazil has been refined by least-squares from single crystal *X*-ray data to an unweighted R value of 0.060 and a weighted R value of 0.070. The Ibitiara pyrophyllite is a 1*Tc* polytype having space group symmetry of $C\bar{1}$. Average bond lengths are Al–O 1.912, Si(1)–O 1.617, and Si(2)–O 1.618Å. The tetrahedral rotation angle (α) is 10.2°, the octahedral flattening angle (ψ) is 57.1° and the tetrahedral thickness angle (τ) is 109.4°. The results agree closely with the structural determination from X-ray powder data of Wardle and Brindley (1972).

Formulae to calculate the apical oxygen separation are derived in order to determine the magnitude of the effects of four geometric parameters: (a) the tetrahedral rotation angle, (b) the octahedral flattening angle, (c) the deviation of the apical oxygen from a mean O_{Apical}–T–O_{basal} angle and (d) the corrugation parameter, Δz. Of these, the corrugation is more effective in adjusting the distance between apical oxygens to provide linkage between the tetrahedral and octahedral sheets and to allow readjustments around the larger vacant site.

Introduction

Earlier work on pyrophyllite has shown it to exist in three polytypic forms: a two layer monoclinic (2*M*), a one layer triclinic (1*Tc*) and a disordered form (Gruner, 1934; Zvyagin, *et al.*, 1969; and Brindley and Wardle, 1970). Rayner and Brown (1965) studied a partially disordered pyrophyllite–2*M* single crystal for lack of better material. Later, powder data were analyzed from the one layer form by Wardle and Brindley (1972) to establish the ideal structure and then to refine the results partially. These results confirmed the earlier model of Zvyagin, *et al.* (1969). Due to the difficulty in obtaining well-crystallized material and the fine-grained nature of pyrophyllite, a detailed single crystal study has not been possible previously.

A single crystal *X*-ray refinement of the structure of pyrophyllite–1*Tc* has been undertaken using material from a recently discovered extensive deposit near Ibitiara, Bahia, Brazil. The crystals appear to be hydrothermal in origin; a thin section of the matrix material shows crystallization of pyrophyllite occurring in vugs, veins, and other openings. Crystals range in size up to 5 cm. Although a detailed study of this deposit has not been made, pyrophyllite–1*Tc* has been shown by synthesis work to form at 375°C and above, whereas the 2*M* variety forms at lower temperature (Eberl, 1979).

Experimental

The crystal chosen for analysis measured originally 5 × 1 × 1 cm and was elongate parallel to the *a* axis. Portions were stained reddish brown from iron oxides, but large sections were pearly white to pale yellow. Material was cleaved from the white/yellow portions and then cut to size with a razor blade. These crystals were quite sensitive to solvents such as acetone and would partially split along cleavage upon drying. Furthermore, slight pressure caused the platelets to bend. Seventy sections were examined by the precession method and one, approximately rectangular in shape and 0.6 × 0.5 × 0.05 mm in size, was chosen for further study. This crystal, mounted so that the b^* axis was parallel to the fiber length, was glued along the fiber for support. The composition of a nearby crystal was determined by wet chem-

[1]Present address: Department of Geological Sciences, University of Michigan, Ann Arbor, Michigan 48109.

0003–004X/81/0304–0350$02.00

Table 1. Chemical analysis of pyrophyllite from Ibitiara, Brazil

Oxides	[a]Weight percent	Cations per 22 positive charges		
SiO_2	66.04	Si	3.976	4.000^{IV}
Al_2O_3	28.15	Al	0.024	
Fe_2O_3	0.64		1.974	
MgO	0.04	Fe^{3+}	0.029	2.007^{VI}
MnO	[b]b.d.	Mg	0.004	
Na_2O	0.04	Na	0.005	0.006
K_2O	b.d.	Ca	0.001	
CaO	0.01			
H_2O+	5.27			
H_2O-	b.d.			
Sum of Oxides	100.19			

[a]Wet chemical analysis by Jun Ito, Dept. of Geophysical Sciences, University of Chicago.

[b]below detection

ical analysis (Table 1) and corresponds to $Al_{1.97}Fe^{3+}_{0.03}(Si_{3.98}Al_{0.02})\ O_{10}\ (OH)_2$.

Precession photographs indicated that the sample is triclinic with systematic absences of the type $h + k \neq 2n$ for general reflections indicating a C centered lattice and space group $C1$ or $C\bar{1}$. Space group $C\bar{1}$ was used for the refinement. Reflections showed splitting and elongation of the type expected where there is small but partial separation along cleavage planes; however, the crystal was clearly superior to the others. No streaking was observed on the Okl net parallel to Z^* indicating that the crystal was ordered.

Data were collected on a Picker FACS-1 four circle automated diffractometer (Lenhert, 1975) using a graphite monochromator with molybdenum radiation. Unit cell parameters as determined by least-squares refinement of fifteen high-angle, hand-centered reflections were $a = 5.160(2)$, $b = 8.966(3)$, $c = 9.347(6)$Å, $\alpha = 91.18(4)$, $\beta = 100.46(4)$, $\gamma = 89.64(3)°$. 3214 non-zero reflections were collected using the stationary counter, moving crystal technique in the continuous ω scan mode (at 1°/min, 2.5° peak width, 20 sec. per background measurement) for the entire reciprocal sphere. The sin θ/λ limitations were 0.81 Å^{-1} for half the sphere ($h = -8$ to 8, $k = 0$ to 14 and $l = -14$ to 14) and 0.65 Å^{-1} for the other half ($h = -6$ to 6, $k = -11$ to 0 and $l = -11$ to 11). Three standard reflections were monitored after every 50 reflections to check the crystal and electronic stability. The data were corrected for Lorentz, polarization and absorption effects and then were symmetry averaged to produce 1,574 unique non-zero intensities. Absorption was corrected by comparison to complete ψ scans (10° increments in ϕ) for selected reflections spaced at 2θ intervals of approximately 5°. In this way, absorption effects caused by the glass fiber also could be considered. A maximum intensity decrease of 62% was observed for some ψ scan data.

Integrated intensities were calculated from the expression $I = [c–0.5\ (t_c/t_b)(B_1 + B_2)]$ where c is the total integrated counts in time t_c, whereas B_1 and B_2 are the background counts in time t_b. The standard deviation of the intensity is given by $\sigma(I) = [c + 0.25\ (t_c/t_b)^2(B_1 + B_2) + (pI)^2]^{1/2}$ where p was chosen arbitrarily as 0.03. Any intensity measured to be less than three times the standard deviation was considered to be zero.

Initial atomic coordinates were obtained for refinement from Wardle and Brindley (1972). The R_1 value ($R_1 = \sum||F_o| - |F_c||/\sum|F_o|$) rapidly dropped from .208 to .089 when atomic coordinates and then isotropic temperature factors were varied. Thirty one reflections that showed excessive splitting in Weissenberg and precession photographs were eliminated from the refinement and, after varying the anistropic thermal parameters, R_1 decreased to 0.060 and R_2 ($R_2 = [\sum w(|F_o| - |F_c|)^2/\sum w|F_c|^2]^{1/2}$) to 0.070. All correlation coefficients were within the range of ±0.40 and most were quite close to zero. A difference map computed after refinement did not reveal the position of the hydrogen atom. A close estimate of the hydrogen position may be made by varying the positional parameters of hydrogen within crystal-chemically reasonable values until the minimum electrostatic energy is determined (Baur, 1965). By following such a procedure, Giese (1973) determined the coordinates of the hydrogen as (0.148, 0.104, 0.159) for the model determined by Wardle and Brindley (1972). The hydrogen location of (0.1533, 0.1107, 0.1541) has been determined by repositioning the hydrogen by the amount of deviation observed in the nearest neighbor oxygen between this refinement and that reported by Wardle and Brindley. However, the hydrogen coordinates derived in this manner were not used in the refinement process. Tables 2–4 list observed and calculated structure amplitudes[2], final atomic coordinates and calculated bond lengths and angles. The crystallographic least-squares program, ORFLS (Busing, Martin and Levy, 1962), the crystallographic function program, ORFFE (Busing, Martin and Levy, 1964), and the bond distance and angle program, SA-

[2]To obtain a copy of Table 2, order Document AM-81-155 from the Business Office, Mineralogical Society of America, 2000 Florida Ave., N.W., Washington, D.C. 20009. Please remit $1.00 in advance for microfiche.

Table 3. Final atomic parameters

Atom	x	y	z	$B_{refined}$	$^*\beta_{11}$	β_{22}	β_{33}	β_{12}	β_{13}	β_{23}
Al	0.4995(2)**	0.16705(9)	-0.00008(9)	0.70(2)	0.0053(3)	0.00165(8)	0.00298(8)	-0.0005(1)	0.0006(1)	-0.00006(6)
Si(1)	0.7449(2)	-0.00303(8)	0.29169(8)	0.68(2)	0.0057(2)	0.00160(7)	0.00289(7)	-0.0009(1)	0.0006(1)	0.00001(5)
Si(2)	0.7595(2)	0.32577(8)	0.29230(8)	0.70(2)	0.0057(2)	0.00162(7)	0.00309(7)	-0.0008(1)	0.0009(1)	-0.00008(5)
O(1)	0.6495(4)	0.0018(2)	0.1155(2)	0.89(4)	0.0082(6)	0.0023(2)	0.0031(2)	-0.0004(3)	0.0002(3)	-0.0001(1)
O(2)	0.7314(4)	0.3079(2)	0.1158(2)	0.84(4)	0.0068(6)	0.0026(2)	0.0030(2)	-0.0008(3)	0.0006(3)	-0.0002(1)
OH	0.2263(4)	0.1927(2)	0.1081(2)	1.00(4)	0.0080(7)	0.0029(2)	0.0038(2)	0.0005(3)	0.0012(3)	0.0005(2)
Ob(1)	0.0498(4)	0.3891(2)	0.3589(2)	0.95(4)	0.0078(6)	0.0027(2)	0.0039(2)	-0.0021(3)	0.0006(3)	0.0002(1)
Ob(2)	0.7251(5)	0.1637(2)	0.3584(2)	0.95(4)	0.0113(7)	0.0017(2)	0.0039(2)	-0.0008(3)	0.0017(3)	-0.0001(1)
Ob(3)	0.5452(4)	0.4426(2)	0.3325(2)	1.01(4)	0.0061(6)	0.0031(2)	0.0042(2)	0.0002(3)	0.0007(3)	-0.0007(2)

* The anisotropic temperature factor form is exp $(-\Sigma_i\Sigma_j\beta_{ij}h_ih_j)$

** Values in parenthesis represent estimated standard deviations (esd) in terms of the least units cited for the value to the immediate left, thus 0.4995(2) indicates an esd of 0.0002.

DIAN69 (Baur and Wenninger, unpublished) were used in the course of the work.

Discussion

The results presented are in close agreement with the structural determination of Wardle and Brindley (1972). When the mean tetrahedral bond lengths are compared to the mean bond distance of 1.608 for pure silicon (Hazen and Burnham, 1973), it is apparent that the tetrahedral sites lack significant cation substitution in accord with the chemical analysis. Within the precision of the determination, a comparison of tetrahedra show uniformity in size and shape with only the very slightest of deviations when O_b–O_b distances and O_b–T–O_b angles are compared. The Al–O distances within the octahedral site also are uniform as are the two Al–(OH) distances. A projection of the structure down [001] is shown in Figure 1.

Cation to apical oxygen distances are significantly longer than T–O_b distances. Takéuchi (1975) has shown that tetrahedra in layer silicates tend to elongate along [001], particularly for dioctahedral structures rich in silicon. However, the predicted value of the cation to apical oxygen distance of 1.615Å as calculated from equations derived by Baur (in press) indicate a deviation (0.018Å) greater in magnitude than what might be reasonably expected. Since the thermal parameters (see below) also appear affected along [001], the reported standard deviations associated with the *z* atomic coordinates may be too low.

The pyrophyllite structure is not directly com-

Table 4. Interatomic distances and angles

	Bond length (Å)			Bond angles (°)	
		Tetrahedron Si(1)			
O(1)	1.632(2)*	O(1)--Ob(1)	2.643(3)	O(1)--Ob(1)	108.9(1)
Ob(1)	1.615(2)	Ob(2)	2.639(3)	Ob(2)	108.5(1)
Ob(2)	1.618(2)	Ob(3)	2.663(3)	Ob(3)	110.7(1)
Ob(3)	1.602(2)	Ob(1)--Ob(2)	2.628(3)	Ob(1)--Ob(2)	108.7(1)
Mean	1.617	Ob(3)	2.660(3)	Ob(3)	111.5(1)
		Ob(2)--Ob(3)	2.608(3)	Ob(2)--Ob(3)	108.1(1)
		Mean	2.640	Mean	109.4
		Tetrahedron Si(2)			
O(2)	1.634(2)	O(2)--Ob(1)	2.643(3)	O(2)--Ob(1)	108.7(1)
Ob(1)	1.616(2)	Ob(2)	2.639(3)	Ob(2)	108.6(1)
Ob(2)	1.614(2)	Ob(3)	2.660(3)	Ob(3)	110.3(1)
Ob(3)	1.607(2)	Ob(1)--Ob(2)	2.633(3)	Ob(1)--Ob(2)	109.2(1)
Mean	1.618	Ob(3)	2.613(3)	Ob(3)	108.3(1)
		Ob(2)--Ob(3)	2.662(3)	Ob(2)--Ob(3)	111.5(1)
		Mean	2.642	Mean	109.4
				Si(1)--Ob(1)--Si(2)	131.5(1)
				Si(1)--Ob(2)--Si(2)	131.8(1)
				Si(1)--Ob(3)--Si(2)	144.7(1)
				Mean	136.0
		Octahedron Al			
O(1)	1.926(2)	O(1)--O(2)	2.780(3)	O(1)--O(2)	92.52(9)
$O(1)^a$	1.922(2)	$O(2)^b$	2.934(3)	$O(2)^b$	99.24(9)
O(2)	1.922(2)	OH	2.758(3)	OH	92.60(9)
$O(2)^b$	1.926(2)	$O(1)^a$--$O(2)^b$	2.779(3)	$O(1)^a$--$O(2)^b$	92.53(9)
OH	1.889(2)	OH	2.853(3)	OH	96.96(9)
OH^b	1.888(2)	OH^b	2.798(3)	OH^b	94.53(9)
Mean	1.912	O(2)--OH	2.798(3)	O(2)--OH	94.52(9)
		OH^b	2.857(3)	OH^b	97.15(9)
		$O(2)^b$--OH^b	2.761(3)	$O(2)^b$--OH	92.77(9)
		Mean (unshared)	2.813	Mean (unshared)	94.76
		$O(1)$--$O(1)^a$	2.415(3)	$O(1)$--$O(1)^a$	77.74(9)
		$O(2)$--$O(2)^b$	2.420(3)	$O(2)$--$O(2)^b$	77.95(8)
		OH--OH^b	2.338(3)	OH--OH^b	76.52(9)
		Mean (shared)	2.391	Mean (shared)	77.40

[a] (-x,-y,-z)

[b] (1/2-x,1/2-y,z)

*Values in parentheses represent the estimated standard deviation (esd) in terms of the least units cited for the value to the immediate left, thus 1.632(2) indicates an esd of 0.002

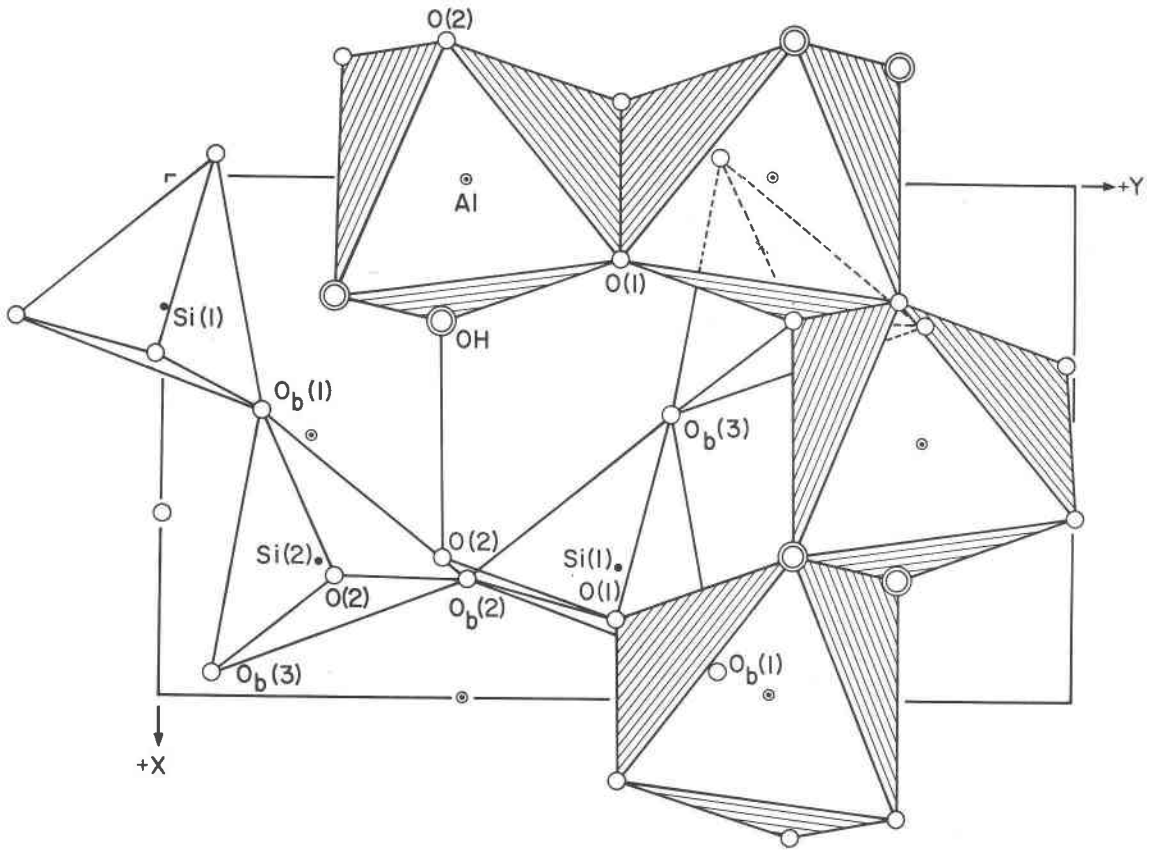

Fig. 1. The unit cell of pyrophyllite-1*Tc* projected down *Z*. One tetrahedral sheet is not shown and portions of the octahedral sheet have not been illustrated to simplify the projection. The vacant octahedral site is located near the center of the figure. The apparent difference in tilt of the two tetrahedra is a result of the β angle.

parable in all respects to the dioctahedral mica structures because the manner of stacking is not identical. Adjacent 2:1 layers in mica must coordinate so the hexagonal silicate rings exactly superimpose around the interlayer cation. In contrast, pyrophyllite does not have an interlayer cation and, thus, successive layers are not constrained to such positions. Basal oxygens of one layer superimpose between the basal oxygens of the hexagonal ring of the adjacent layer. This arrangement creates an offset approximately parallel to the [$\bar{1}$10] or, more precisely, along the resultant of $-0.14a$ along *X* and $0.16b$ along *Y*. The stacking arrangement produces not only the triclinic symmetry but also accounts for the deviation of the unit-cell parameters, α and γ, from 90°. Zvyagin *et al.* (1969) suggest that stacking may be stabilized because such an arrangement minimizes Si—Si repulsion between layers since the silicons are staggered across the interlayer region.

In 2:1 layer silicates, distortions from an ideal hexagonal tetrahedral sheet arise when the larger tetrahedral sheet reduces its lateral dimensions to compensate for the smaller lateral size of the octahedral sheet. Alternatively, the octahedral sheet may expand its lateral dimensions to partly compensate for this misfit. Table 5 gives the structural distortions that describe these compensating effects. The differences in sizes of the tetrahedral and octahedral sheets are adjusted by 1) a rotation (α) of tetrahedra in (001) resulting in a ditrigonal tetrahedral ring, 2) a thickening of the tetrahedra (τ), and 3) a flattening of the octahedra (ψ) to lengthen the octahedral edges. A fourth structural distortion, Δz, may be described as a corrugation of basal oxygens along [110] which results in a tilt of the tetrahedra out of (001). Such an effect is found only in 2:1 layer silicates with the M(1) octahedral site larger than M(2). This effect allows for a small lengthening of the distance between apical oxygens around the vacant or larger M(1) site. In this way the M(1) site increases in size to accommodate the larger cation or vacancy.

These geometrical considerations may be used to

describe fully the atomic adjustment required to minimize the tetrahedral/octahedral misfit. The important distances for consideration are those that involve anions common to both sheets, namely the apical oxygen separations. The measured apical oxygen separation from O(1) to O(2) across $O_b(2)$ is 2.780(3)Å and across $O_b(1)$ is 2.779(3)Å. The third apical oxygen separation, O(1) to O(2) across $O_b(3)$, is 3.460(3)Å which is significantly larger than the other two equal distances because of the sense of out-of-plane twist resulting from the Δz distortion. Hence, the formulae presented below apply only to the apical oxygen separation across $O_b(1)$ and $O_b(2)$. However, it may be shown through analogous derivations that the four geometrical factors also account for the larger distance. Calculations involving the formulae given below show the effects of the distortions and may be used to understand the relative importance of each.

It is well known that tetrahedral rotation reduces the lateral dimensions of the tetrahedral sheet. In pyrophyllite and other layer silicates which have tetrahedral faces that may be nearly described as equilateral triangles, the resulting distance between apical oxygens, AO_α, may be calculated from:

$$AO_\alpha = [2(e_{tet})\cos\alpha]/\sqrt{3} \qquad (1)$$

where e_{tet} is the average measured tetrahedral edge length. In pyrophyllite, the tetrahedral edge length is 2.641Å and α is 10.2° resulting in the apical oxygen separation of 3.00Å. This represents a 0.05Å shortening from the ideal hexagonal silicate ring arrangement (AO_{ideal}) of 3.05Å.

The corrugation effect (Fig. 2) produces an out-of-plane twisting of tetrahedra about the bridging basal oxygen for the tetrahedra in the [110] tetrahedral chain and a shortening of the distance between apical oxygens along the octahedral edge parallel to (001). The maximum shortening possible occurs at a twisting angle of 19.5° when the faces formed by the two basal oxygens, $O_b(1)$ and $O_b(2)$, and the apical oxygen of each tetrahedron become vertical. At the maximum twist of 19.5° the apical oxygen separation is the same as the ideal tetrahedral edge length. The magnitude of twist or tilt is determined by the amount (Δz) the basal oxygens deviate from an average basal plane and, for pyrophyllite, is 6.0°.

The mean of the three O_{apical}–T–O_{basal} values, τ, is a measure of the thickness of the tetrahedron. For 2:1 layer silicates, tetrahedra are elongated along the Z direction and compressed within (001), thereby producing a τ parameter greater in value than the ideal of 109.47°. Compression within (001) further reduces the lateral dimensions of a larger tetrahedral sheet to allow for the lack of fit between unrestrained octahedral and tetrahedral sheets. In pyrophyllite, the τ value of 109.4 is very close to the ideal value. This indicates that the nearly pure Si tetrahedral sheet does not require as much compression within (001) as layer silicates with increased Al substitution causing larger lateral tetrahedral sheet dimensions. However, it should be noted that τ is an average of three values, one significantly larger (approximately 110.5°) than the other two (each approximately 108.7°). The consequence of this one larger angle is that the apical oxygen is shifted nearly parallel to (001) approximately toward the coordinating anion on the shared octahedral edge. The movement is in the same direction as that produced by the corrugation effect but significantly, only the apical oxygen adjusts its position. This trend is observed in all 2:1 dioctahedral micas as well, and may be a result of repulsions of adjacent Al^{3+} in the octahedral site since the direction of movement of the apical oxygen is similar to that produced by a shortened shared edge. Lending credence to this interpretation is the fact that a similar trend is not observed in trioctahedral micas. In this case, cation charges of each octahedral site are

Table 5. Structural features of pyrophyllite

Parameter	Value
[a] α_{tet}(°)	10.2
[b] τ_{tet}(°)	109.4
[d] β_{ideal}(°)	100.60
[c] ψ_{oct}(°)	57.1
Sheet thickness (Å)	
tetrahedral	2.153
Octahedral	2.079
Interlayer separation (Å)	2.759
Basal oxygen Δz_{ave}(Å)	0.240

[a] Tetrahedral rotation is calculated from α = 1/2|120° - mean Ob-Ob-Ob angle|.

[b] The tetrahedral angle is defined as $\tau = O_{apical}$--Si--O_{basal}. The ideal value is 109.47°.

[c] The mean octahedral angle, ideally 54.73°, is calculated from cosψ = oct. thickness/2(M--O,OH).

[d] $\beta_{ideal} = 180° - \cos^{-1}(\underline{a}/3\underline{c})$.

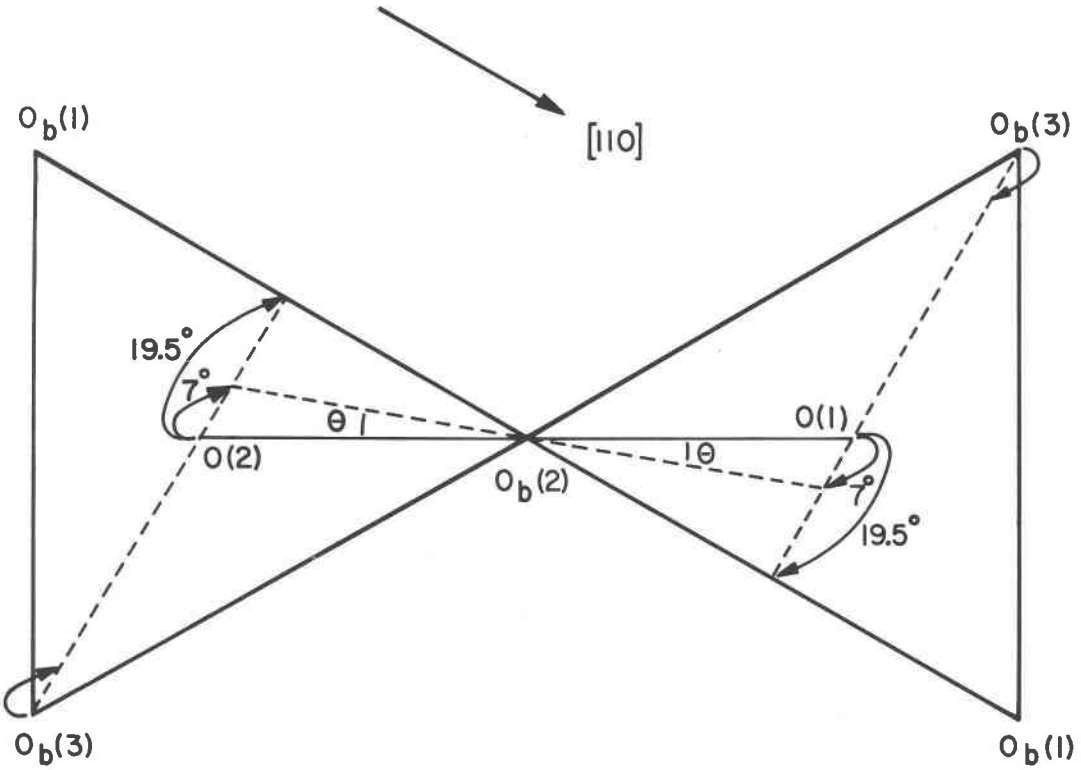

Fig. 2. Idealized Si(1) and Si(2) tetrahedra (without tetrahedral rotation (α) effects) projected onto a plane parallel to the plane established by the basal oxygens. The direction of tilt or twist produced by the corrugation effect is shown (see text for additional explanation).

pulling the apical oxygen from three sides; each attractive force is approximately 120° apart.

Since the direction of apical oxygen shift from both the corrugation effect and the non-equal nature of the three O_{apical}–T–O_{basal} angles is similar, both effects may be calculated from the following formula:

$$AO_\theta = (AO_{ideal})(\sqrt{3}\cos\alpha)/2\cos(30° - \theta) \quad (2)$$

where theta is defined as

$$\theta = 30° - \tan^{-1}\left(\frac{1}{\sqrt{3}} - \frac{\gamma}{19.5\sqrt{3}}\right) \quad (3)$$

The tilt angle, γ, represents the angular deviation of the tetrahedron from the basal plane with the apical oxygen as reference; it is the cumulative angle resulting from the corrugation effect and the unequal O_{apical}–T–O_{basal} angles. Note that the effects from tetrahedral rotation, α, are included in equation 2. Also, note that θ is the angle (Fig. 2) shown *in projection* on the (001) plane whereas γ is the actual angle of tilt (not shown). In pyrophyllite, γ is equal to 7°, 6° caused by the corrugation effect and the remainder from the difference of 110.5° from the ideal τ value of 109.5°. Theta is equal to 9.7° and AO_θ is calculated to equal 2.77Å (*vs.* 2.78Å observed). In addition to the shortening of 0.05Å caused by tetrahedral rotation, the above formulae may be used for individual effects to show that the larger O_{apical}–T–O_{basal} angle reduces the distance by 0.04Å and the corrugation effect reduces the distance by approximately 0.19Å. The above formulae 2 and 3 are only approximations since the locus of points forming an arc by the rotating apical oxygen is described in the derivation of formula 3 as a straight line. However, these effects do not decrease the overall lateral tetrahedral sheet dimensions, but allow readjustments around the vacant site. Clearly, the corrugation effect plays the major role in these readjustments.

The structural parameters listed in Table 5 are consistent with parameters derived from the results of accurate refinements made of the dioctahedral micas. The mean octahedral angle, ψ, is significantly smaller than calculated values from any previous muscovite refinement, however the chemical occupancy of the octahedral site for each of these muscovites has not been pure aluminum. The ψ parame-

ter and octahedral sheet thickness are identical to those of margarite (Guggenheim and Bailey, 1978), which has an octahedral composition closer to the Ibitiara pyrophyllite.

Thermal ellipsoids

Magnitudes and orientations of apparent atomic vibration ellipsoids are given in Table 6. The ellipsoids are quite large in magnitude and considerably elongate nearly parallel to the crystallographic Z direction. The r_3/r_1 ratio for all atoms is approximately 1.6 with ratios of approximately 1.6 for the cations, 1.3 for the apical oxygens and OH, and 1.7 for the basal oxygen atoms. Similar magnitudes and anisotropy have been observed for other layer silicates refined from single crystal diffractometer data (*e.g.*, Hazen and Burnham, 1973; Guggenheim and Bailey, 1977). For these structures, such apparent thermal motions have been attributed to local variations in atomic position. However, in contrast to these structures, pyrophyllite does not have significant amounts of tetrahedral Al. It is the differences in bond lengths between tetrahedral Al and Si and the lack of tetrahedral cation order that has been suggested as the cause of such anisotropy and magnitude. Clearly, such reasoning cannot be used to explain the apparent vibration ellipsoids in pyrophyllite, nor is it probable that such large, anisotropic ellipsoids are due to thermal vibration alone.

Both the large magnitudes and ellipsoid elongation parallel to the c axis may be explained by small and random displacements of the 2:1 layer unit along the Z direction. Such an explanation is certainly consistent with the very weak bonding between layers. Kodama, *et al.* (1971) observed weak diffuse scattering from pyrophyllite in electron microdiffraction and monochromatic X-ray diffraction patterns. Kodama (1977) interpreted the diffuse streaking as indicating some type of semi-random periodicity along [100], [$\bar{1}$10] and [110]. These directions coincide with chains of tetrahedra in the silicate sheet. Kodama suggested that thermal vibrations and small displacements of atoms due to out-of-plane distortions of the anion framework could account for the diffuse scattering they observed. Although there was a moderate intensity spread at each Bragg reflection caused by the mosaic character of the crystal, no diffuse scattering was obvious in the Ibitiara specimen and long exposures were not attempted. However, the atomic displacements causing the ellipsoid elongation as discussed above would contribute to the diffuse scattering in the directions observed by Kodama, *et al.*

Table 6. Magnitudes and orientations of apparent thermal ellipsoids

Atom	Axis	rms (Å) displacement	Angle (°) with respect to X	Y	Z
Al	r_1	0.075(2)*	48(6)	42(6)	91(2)
	r_2	0.089(2)	43(6)	132(6)	95(3)
	r_3	0.113(2)	96(3)	94(2)	5(3)
Si(1)	r_1	0.069(2)	51(3)	39(3)	92(2)
	r_2	0.095(2)	41(3)	129(3)	87(4)
	r_3	0.112(1)	102(3)	88(3)	4(3)
Si(2)	r_1	0.072(2)	51(4)	39(4)	93(2)
	r_2	0.093(2)	39(4)	129(4)	99(3)
	r_3	0.115(1)	92(3)	95(2)	9(3)
O(1)	r_1	0.093(4)	61(14)	33(17)	80(7)
	r_2	0.104(4)	44(14)	123(17)	73(11)
	r_3	0.121(4)	120(9)	90(7)	20(10)
O(2)	r_1	0.087(5)	38(9)	55(8)	85(6)
	r_2	0.108(4)	52(9)	140(12)	106(21)
	r_3	0.115(3)	95(14)	107(17)	17(20)
OH	r_1	0.099(4)	29(21)	117(20)	91(9)
	r_2	0.108(4)	119(21)	146(17)	67(7)
	r_3	0.130(3)	89(6)	72(7)	23(7)
Ob(1)	r_1	0.075(5)	43(4)	47(4)	95(3)
	r_2	0.120(4)	58(7)	127(7)	60(12)
	r_3	0.133(3)	116(8)	67(8)	31(12)
Ob(2)	r_1	0.080(5)	77(5)	13(5)	91(4)
	r_2	0.119(4)	26(12)	101(5)	123(14)
	r_3	0.131(3)	68(13)	97(4)	33(14)
Ob(3)	r_1	0.089(5)	12(7)	100(10)	94(5)
	r_2	0.105(4)	97(11)	152(6)	114(4)
	r_3	0.140(3)	100(3)	116(4)	24(4)

* Values in parenthesis represent the estimated standard deviation (esd) in terms of the least units cited for the value to the immediate left, thus 0.075(2) indicates an esd of 0.002.

Poorly crystalline material studied by Kodama, *et al.* could enhance the effect along these directions and incipient cleavage could mask the effect along c^*.

Rosenberg (1974) suggested that any tetrahedral substitution of Al^{3+}, not balanced by small substitutions in the octahedral sheet, could be charge compensated by H^+ associated with the basal oxygen plane causing a change in basal spacing. Furthermore, even if the compensating H^+ is associated with an apical oxygen, Giese (1975) has shown that an imbalance in charge would also affect interlayer spacing. Although the Ibitiara pyrophyllite has only a small amount of tetrahedral aluminum, such an explanation is plausible also for producing random atomic displacements along Z.

As noted above, the r_3/r_1 ratio of the cations exceeds that of the apical oxygens. This indicates a greater apparent electron distortion around the highly charged cations than around the apical oxygens. Such a distortion is not physically plausible. Since there was considerable difficulty in obtaining a

suitable crystal for study, a compromise in crystal quality (see Experimental section) was made. However, similar effects are also observed in phlogopite (Hazen and Burnham, 1973) for data collected by similar methods and on apparently higher quality material. It is well known that any effects not explicitly accounted for in the data will affect the thermal parameters. Therefore, caution should be exercised in reaching conclusions explaining these apparent thermal vibrations.

Acknowledgments

We gratefully acknowledge the late Jun Ito for the wet chemical analysis and thank Dr. Paul Moore of the University of Chicago for the pyrophyllite sample. We also thank Dr. Werner H. Baur of the University of Illinois at Chicago for fruitful discussions and Dr. S. W. Bailey of the University of Wisconsin-Madison and Dr. R. F. Giese, Jr. of the State University of New York at Buffalo for reviewing the manuscript. The Computer Center of the University of Illinois at Chicago supplied computing time.

References

Baur, W. H. (1965) On hydrogen bonds in crystalline hydrates. Acta Crystallographica 19, 909–916.

Baur, W. H. (1980) Interatomic distance predictions for computer simulation of crystal structures. In M. O'Keefe and A. Navrotsky, Eds., Structure and Bonding in Crystals, Academic Press, New York, in press.

Brindley, G. W. and Wardle, R. (1970) Monoclinic and triclinic forms of pyrophyllite and pyrophyllite anhydride. American Mineralogist 55, 1259–1272.

Busing, W. R., Martin, K. O., and Levy, H. A. (1962) ORFLS, a Fortran crystallographic least-squares refinement program. U. S. National Technical Information Service ORNL-TM-305.

Busing, W. R., Martin, K. O., and Levy, H. A. (1964) ORFFE, a Fortran crystallographic function and error program. U. S. National Technical Information Service ORNL-TM-306.

Eberl, D. (1979) Synthesis of pyrophyllite polytypes and mixed layers. American Mineralogist 64, 1091–1096.

Giese, R. F., Jr. (1973) Hydroxyl orientation in pyrophyllite. Nature Physical Science 241, 151.

Giese, R. F., Jr. (1975) Interlayer bonding in talc and pyrophyllite. Clays and Clay Minerals 23, 165–166.

Gruner, J. W. (1934) The crystal structures of talc and pyrophyllite. Zeitschrift Kristallographica 55, 412–419.

Guggenheim, S. and Bailey, S. W. (1977) The refinement of zinnwaldite-1M in subgroup symmetry. American Mineralogist 62, 1158–1167.

Guggenheim, S. and Bailey, S. W. (1978) The refinement of the margarite structure in subgroup symmetry: correction, further refinement, and comments. American Mineralogist 63, 186–187.

Hazen, R. M. and Burnham, C. W. (1973) The crystal structures of one layer phlogopite and annite. American Mineralogist 58, 889–900.

Kodama, H. (1977) An electron-diffraction study of a microcrystalline muscovite and its vermiculized products. Mineralogical Magazine 41, 461–468.

Kodama, H., Alcover, J. F., Gatineau, L. and Méring, J. (1971) Diffusions anormales (rayons X et electrons) dans les phyllosilicates 2:1. (abstr.) Structure and Surface Properties of Clay Minerals Symposium.

Lenhert, P. G. (1975) An adaptable disk-oriented automatic diffractometer control program. Journal of Applied Crystallography 8, 568–570.

Rayner, J. H. and Brown, G. (1965) Structure of pyrophyllite. Clays and Clay Minerals. Proceedings of the 13th National Clay Conference in Madison, WI, 73–84.

Rosenberg, P. E. (1974) Pyrophyllite solid solutions in the system Al_2O_3–SiO_2–H_2O. American Mineralogist 59, 254–260.

Takéuchi, Y. (1975) The distortion of Si (Al)-tetrahedra in sheet silicates. Contributions to Clay Mineralogy. Sudo Volume, 1–6.

Wardle, R. and Brindley, G. W. (1972) The crystal structures of pyrophyllite-1*Tc*, and of its dehydroxylate. American Mineralogist 57, 732–750.

Zvyagin, B. B., Mishchenko, K. S., and Soboleva, S. V. (1969) Structures of pyrophyllite and talc in relation to the polytypes of mica-type minerals. Soviet Physics-Crystallography 13, 511–515.

Manuscript received, July 24, 1980;
accepted for publication, December 4, 1980.